Design, Synthesis and Characterization of a PEGylated Stanozolol for Potential Therapeutic Applications

Cristian Vergallo, Giulia Torrieri, Riccardo Provenzani, Sini Miettinen, Karina Moslova, Markku Varjosalo, Maria Chiara Cristiano, Massimo Fresta, Christian Celia, Hélder A. Santos, Felisa Cilurzo, Luisa Di Marzio

PII: S0378-5173(19)30871-3
DOI: https://doi.org/10.1016/j.ijpharm.2019.118826
Reference: IJP 118826

To appear in: *International Journal of Pharmaceutics*

Received Date: 29 May 2019
Revised Date: 22 October 2019
Accepted Date: 25 October 2019

Please cite this article as: C. Vergallo, G. Torrieri, R. Provenzani, S. Miettinen, K. Moslova, M. Varjosalo, M. Chiara Cristiano, M. Fresta, C. Celia, H.A. Santos, F. Cilurzo, L. Di Marzio, Design, Synthesis and Characterization of a PEGylated Stanozolol for Potential Therapeutic Applications, *International Journal of Pharmaceutics* (2019), doi: https://doi.org/10.1016/j.ijpharm.2019.118826

Design, Synthesis and Characterization of a PEGylated Stanozolol for Potential Therapeutic Applications

Cristian Vergallo[a], Giulia Torrieri[b], Riccardo Provenzani[b], Sini Miettinen[c], Karina Moslova[d], Markku Varjosalo[c], Maria Chiara Cristiano[e], Massimo Fresta[e], Christian Celia[a,*], Hélder A. Santos[b,f,*], Felisa Cilurzo[a,*], Luisa Di Marzio[a]

[a]Department of Pharmacy, University of Chieti - Pescara "G. d'Annunzio", Via dei Vestini 31, I-66100, Chieti, Italy.

[b]Drug Research Program, Division of Pharmaceutical Chemistry and Technology, Faculty of Pharmacy, University of Helsinki, FI-00014, Helsinki, Finland.

[c]Institute of Biotechnology, University of Helsinki, FI-00014, Helsinki, Finland.

[d]Department of Chemistry, University of Helsinki, FI-00014, Helsinki, Finland.

[e]Department of Health Sciences, University of Catanzaro "Magna Graecia", Via "S. Venuta" s.n.c., I-88100, Catanzaro, Italy.

[f]Helsinki Institute of Life Science (HiLIFE), University of Helsinki, FI-00014, Helsinki, Finland.

Corresponding authors: *e-mail: c.celia@unich.it (Christian Celia); *e-mail: helder.santos@helsinki.fi (Hélder A. Santos); *e-mail: felisa.cilurzo@unich.it (Felisa Cilurzo).

Keywords: PEGylation, Polyethylene Glycol (PEG) derivatives, Biopolymers, Conjugated Drug Delivery Systems, Stanozolol.

Abstract

Stanozolol (STZ) is a drug used to treat serious disorders like aplastic anemia and hereditary angioedema. It is also indicated as an adjunct therapy for the treatment of vascular disorders and growth failures. Encouraging results obtained using animal models demonstrated that STZ increases bone formation and mineralization, thus improving both density and biomechanical properties. Like natural androgens, such as TST and 5α-dihydrotestosterone (5α-DHT), STZ binds androgen receptor (AR) to activate AR-mediated signalling. Despite its therapeutic effects, this synthetic anabolic-androgenic steroid (AAS), or 5α-DHT derivative, due to its high lipophilicity, is poor soluble in water. Thus, to increase the water solubility and stability of STZ, as well as its bioavailability and efficacy, an innovative PEGylated STZ (STZ conjugated with $(MeO\text{-}PEG\text{-}NH_2)_{10kDa}$, $(MeO\text{-}PEG\text{-}NH)_{10kDa}$-STZ) was synthesized. As confirmed by chromatography (RP-HPLC) and spectrometry (ATR-FTIR, ^{1}H-NMR, elemental CHNS(O) analysis, MALDI-TOF/TOF) analyses, a very pure, stable and soluble

compound was obtained. Acetylcholinesterase (AChE) competitive ELISA kit demonstrated that the resulting PEGylated STZ competes against biological TST, especially at lower concentrations. Cytotoxicity of increasing concentrations (1, 10, 25 or 50 μM) of STZ and/or $(MeO\text{-}PEG\text{-}NH)_{10kDa}$-STZ was also evaluated for up 80 h by performing the MTT assay on human osteosarcoma Saos-2 cells, which express AR and are responsive to STZ. PEGylation mitigated cytotoxicity of STZ, by increasing the cell viability values, especially at higher drug concentrations. Furthermore, these results suggest that $(MeO\text{-}PEG\text{-}NH)_{10kDa}$-STZ is a promising and reliable drug to be used in clinical conditions in which TST is required.

1. Introduction

Testosterone (TST) is the predominant androgen, which plays a key role in the growth of the primary male reproductive tissues and organs. This hormone is involved in every step of male sexual response, facilitating the development and maintenance of male secondary sexual traits as well as important functions like spermatogenesis. TST not only affects the male reproductive system, but it is also an essential hormone for women, with physiological actions mediated directly or via aromatisation of oestradiol throughout the body (**Miah et al., 2019**; **Rastrelli et al., 2019**; **Shin et al., 2019**). TST influences muscle mass, bone mineral density (BMD), erythropoiesis, and the activity of many other systems, by including the nervous system, where it plays a significant role in the regulation of mood and cognition (**Bienenfeld et al., 2018**; **Rastrelli et al., 2018**; **Davis and Wahlin-Jacobsen, 2015**). 5α-dihydrotestosterone (5α-DHT) is a biologically active metabolite of the TST hormone. Stanozolol (STZ), or 17α-methyl-2'H-androst-2-eno[3,2-c]pyrazol-17β-ol, is a synthetic derivative of 5α-DHT formed by the condensation of the 3-keto-aldehyde moiety of oxymetholone with hydrazine. Even though this synthetic anabolic-androgenic steroid (AAS) has binding affinity for the androgen receptor (AR) lower than that of the natural androgen TST, it strongly activates AR-mediated signalling (**Feldkoren, and Andersson, 2005**). Structural changes have been made to the TST molecule in order to maximize the anabolic effects and minimize the androgenic ones. Thus, from all compounds belonging to 17 α-alkylated AASs, STZ originates from the substitution of the 17 α-hydrogen on the steroid nucleus for a methyl group. In addition, a pyrazole ring is attached to the A ring of the same steroid nucleus. Alkylation prevents its deactivation by hepatic first-pass metabolism (necessitating hepatic monitoring), which promotes oral activity. Therapeutic uses of STZ include the treatment of aplastic anemia and hereditary angioedema. It has also been indicated as an adjunct therapy for the treatment of vascular disorders and growth failures, which arise as a result of other medical conditions (**National Center for Biotechnology Information, PubChem Database, 2019**). Systemic administration of AASs is providing some encouraging results. Animal models treated with

AASs show an overall increase in bone formation and mineralization, as well as improvements in bone density and biomechanical properties (**Guimarães et al., 2017**; **Donner et al., 2016**; **Liao et al., 2003**). Intra-articular STZ administration induces positive effects on the synovial membrane and cartilage regeneration in osteoarthritis conditions (**Spadari et al., 2013**), and STZ-soaked deproteinized bone grafts increase new bone formation in calvarial critical-size defects (**Ghiacci et al., 2017**). Recently, Ghiacci et al. (2018) demonstrated that STZ promotes the osteogenic commitment of Saos-2 cells, by enhancing the mineralization process and modulating the expression of genes related to osteogenic differentiation (**Ghiacci et al., 2018**). However, STZ has a half-life of 24 h and daily doses of it are necessary in order to maintain appropriate blood levels. Since STZ resembles to 5α-DHT molecule, therefore it cannot be aromatized to oestrogen. In addition, STZ also has a low water and salt retention (**El Osta et al., 2016**). The poor water solubility of STZ decreases its bioavailability, resulting in low efficacy, high inter-individual variability and, consequently, an unpredictable response (**Lemma et al., 2017**; **Fasinu et al., 2011**). To address these issues, herein, an innovative compound consisting of STZ conjugated with α-methoxy-ω-amino PEG having a nominal molecular weight (MW) of 10000 Da [$(MeO\text{-}PEG\text{-}NH_2)_{10kDa}$], $(MeO\text{-}PEG\text{-}NH)_{10kDa}$-STZ, was synthesized. PEGylation using high MW PEGs (≥ 10 kDa) is an important strategy used to increase half-life, reduce renal clearance, and potentially decrease both the immunogenicity and cytotoxicity of therapeutics (**Razzazan et al., 2016**; **Webster et al., 2009**; **Harris and Chess, 2003**). The evaluation by Joint FAO/WHO Expert Committee on Food Additives (JECFA) included PEGs 200, 300, 400, 600, 1000, 1500, 1540, 4000, 6000, 9000 and 10000. JECFA concluded that the acute and short-term studies cover a wide range of animal species and that PEGs have essentially similar toxicity, with toxicity being inverse to their MW (**JECFA, 1980**). These are the reasons why we chose such $(MeO\text{-}PEG\text{-}NH_2)_{10kDa}$. As shown in **Scheme 1**, a STZ molecule, after carbonate activation of its hydroxyl group by 4-nitrophenyl chloroformate, was conjugated to free primary amine group of $(MeO\text{-}PEG\text{-}NH_2)_{10kDa}$ to form the $(MeO\text{-}PEG\text{-}NH)_{10kDa}$-STZ conjugate (Product 2). Reverse phase high performance liquid chromatography (RP-HPLC), attenuated total reflectance-Fourier transform infrared (ATR-FTIR) and proton nuclear magnetic resonance (^{1}H-NMR) spectroscopy, elemental carbon, hydrogen, nitrogen, sulfur and oxygen (CHNS(O)) analysis, matrix-assisted laser desorption/ionization time-of-flight/time-of-flight mass spectrometry (MALDI-TOF/TOF MS), enzyme-linked immunosorbent assay (ELISA) analyses and cytotoxic assessment (3-(4,5-dimethylthiazol-2-yl)-2,5-diphenyltetrazolium bromide, MTT, assay) on human osteosarcoma Saos-2 cells were performed in order to characterize and validate the successful synthesis of a biologically active $(MeO\text{-}PEG\text{-}NH)_{10kDa}$-STZ conjugate (see **Section 2.**).

2. Material and Methods

2.1. Material

The α-methoxy-ω-amino polyethylene glycol with nominal molecular weight (MW) of 10,000 Da, $(MeO\text{-}PEG\text{-}NH_2)_{10kDa}$, was purchased from Iris Biotech GmbH (Marktredwitz, Germany; Product code: PEG1151). Human osteosarcoma Saos-2 cells (ATCC® HTB-85™) and McCoy's 5A medium (ATCC® 30-2007™) were purchased from Sigma-Aldrich (St. Louis, MO, USA). Fetal bovine serum (FBS), trypsin-EDTA (1×) and penicillin-streptomycin solutions were obtained from GIBCO (Thermo Fisher Scientific, Waltham, MA, USA). Chemicals were of analytical grade and provided by Sigma-Aldrich, unless otherwise indicated.

2.2. Methods

2.2.1. Synthesis of stanozolol-4-nitrophenyl-carbonate (Product 1)

To activate Stanozolol (STZ, MW 328.49158 Da), 15 mg of STZ (22.83 mM) and 18.40 mg (45.64 mM) of 4-nitrophenyl chloroformate (MW 201.56396 Da) were dissolved in 2 mL of anhydrous dichloromethane. The reaction was stirred at room temperature (RT) for 3 h in anhydrous condition. The activated STZ (yield 18.6 mg, 76.85%; degree of activation, as calculated from alkaline hydrolysis of fenate ion in NaOH 0.2 N, 95.5%) was filtered through celite, qualitatively analyzed using thin-layer chromatography (TLC), and purified by a silica gel (SiO_2) column (4×12.5 cm) and a chloroform/methanol/mQ water mixture (78.5%: 19.5%: 2%, v/v) as eluent (Retention factor = 0.5).

2.2.2. Synthesis of STZ conjugated with $(MeO\text{-}PEG\text{-}NH_2)_{10kDa}$, $(MeO\text{-}PEG\text{-}NH)_{10kDa}$-STZ (Product 2)

451.9 mg (12.55 mM) of $(MeO\text{-}PEG\text{-}NH_2)_{10kDa}$ and 10 mg (5.63 mM) of Product 1 (MW 493.5946) were dissolved in 3.6 mL of CH_3CN/H_2O (96.66%: 3.33% v/v), pH 8.0 (triethylamine). The reaction was let to proceed for 3 h under continuous stirring. pH was adjusted at 4.5 with 0.2 N HCl, then Product 2 was purified from the excess of 4-nitrophenyl chloroformate and unreacted STZ by extractions with diethyl ether (6×40 mL). The aqueous phase, containing Product 2 and the excess of $(MeO\text{-}PEG\text{-}NH_2)_{10kDa}$ was dried under vacuum, solubilized in 2 mL of $CHCl_3$ and separate on preparative TLC (yield 121 mg, 46%). The absence of free amine in the conjugate was verified spectrophotometrically (Cary® 50 UV-Vis spectrophotometer, Varian, Palo Alto, CA, USA) at 420 nm after 30 min. of reaction by 2,4,6-trinitrobenzenesulfonic acid solution (TNBS) assay, according to Snyder and Sobocinski method (**Snyder and Sobocinski, 1975**).

STZ: ^{1}H-NMR (400 MHz, DMSO-d_6) δ_{ppm} 12.19 (s, 1H, –NH–), 7.22 (s, 1H, C_{19}), 3.00-4.00 (m, (O–CH_2CH_2)O–), 2.50 (m, 2H, C_3), 2.09 (m, 2H, C_6), 1.36 (m, 12H, $C_{4,7,8,11,13\text{-}16}$), 1.08 (s, 3H, C_{22}), 0.84 (m, 2H, $C_{9,10}$), 0.76 (s, 3H, C_{24}), 0.67 (s, 3H, C_{23}).

$(MeO\text{-}PEG\text{-}NH_2)_{10kDa}$: ^{1}H-NMR (400 MHz, DMSO-d_6) δ_{ppm} 3.00-4.00 (m, (O–CH_2CH_2)O–).

$(MeO\text{-}PEG\text{-}NH)_{10kDa}$-STZ: ^{1}H-NMR (400 MHz, DMSO-d_6) δ_{ppm} 7.72 (s, 1H, C_{19}), 5.574 (s, 1H, –NHCO–), 3.00-4.00 (m, (O–CH_2CH_2)O–), 2.50 (m, 2H, C_3), 1.35 (m, 12H, $C_{4,7,8,11,13\text{-}16}$), 0.84 (m, 2H, $C_{9,10}$), 0.76 (s, 3H, C_{24}), 0.67 (s, 3H, C_{23}).

2.2.3. Evaluation of stability and solubility of STZ, $(MeO\text{-}PEG\text{-}NH_2)_{10kDa}$ and $(MeO\text{-}PEG\text{-}NH)_{10kDa}$-STZ stability

STZ, $(MeO\text{-}PEG\text{-}NH_2)_{10kDa}$ and $(MeO\text{-}PEG\text{-}NH)_{10kDa}$-STZ conjugate (1 mg/mL) were incubated at 37 °C for up 80 h in phosphate buffer (PB) buffered at pH 5.8 and 7.4. Sink condition was maintained during the incubation time. Samples of 100 µL were withdrawn at predetermined times. STZ and $(MeO\text{-}PEG\text{-}NH)_{10kDa}$-STZ samples were filtered by using Anotop® 10 LC syringe filter (alumina-based membrane), pore size 0.2 µm (Whatman, Maidstone, UK) and analyzed by RP-HPLC by using a Waters Corp instrument equipped with binary pump and PDA detector, Phenomenex C18 column (Jupiter, 4.6×250 mm; 5 µm), with the UV detector settled at 230 nm. The eluents A and B were H_2O and CH_3OH, plus 0.05% (v/v) of trifluoroacetic acid (TFA) respectively. The elution was performed by the following gradient: from 5% B to 50% B in 5 min., from 50% B to 100% B in 30 min., plateau of B 100% B for 5 min., and from 100% B to 5% B in 5 min. at a flow rate of 0.8 mL/min. To test the stability of samples, the experiment was carried at 37 °C (selected temperature); in fact, PEG aggregates dispersed in water can form hydrophobic helical structures in the range of temperature from 35 to 40 °C as previously reported (**Azri et al., 2012**; **Polik and Burchard, 1983**). In addition, different classes of compounds are highly reactive toward the terminal amino group of the PEG (**Akiyama et al., 2000**). These processes lead to make less available and/or to replace this amino group with other functional groups, respectively. Thus, the time-dependent stability of $(MeO\text{-}PEG\text{-}NH_2)_{10kDa}$ was evaluated indirectly by assessing its free amino group, according to Snyder and Sobocinski method (**Snyder and Sobocinski, 1975**). Briefly, the high chromogenic product generated by the reaction of free amino group of $(MeO\text{-}PEG\text{-}NH_2)_{10kDa}$ with TNBS was assessed spectrophotometrically (Cary® 50 UV-Vis spectrophotometer, Varian, Palo Alto, CA, USA) at 420 nm after 30 min. of reaction.

The solubility of STZ, $(MeO\text{-}PEG\text{-}NH_2)_{10kDa}$ and $(MeO\text{-}PEG\text{-}NH)_{10kDa}$-STZ conjugate was determined by dissolution in mQ water (25 °C, 1 atm). Briefly, 10 mL of mQ water was added to 10 g of compound, then the mixture was filtered by using Anotop® 10 LC syringe filter (alumina-based membrane), pore size 0.2 µm (Whatman, Maidstone, UK), and the filtrate was lyophilized to dryness and weighed.

2.2.4. Attenuated total reflectance-Fourier transform infraRed (ATR-FTIR) spectroscopy

ATR-FTIR was performed by using a Bruker VERTEX 70 series FTIR spectrometer (Bruker Optik GmbH, Ettlingen, Germany) and an ATR sampling accessory (MIRacle, Pike Technology Inc., Iselin, NJ; USA). The ATR-FTIR spectra were recorded in the wavenumber region of 4000-625 cm^{-1} with a spectral resolution of 4 cm^{-1} at RT, using OPUS 5.5 software (Bruker Optik GmbH, Ettlingen, Germany).

2.2.5. Proton nuclear magnetic resonance (^{1}H-NMR) spectroscopy

^{1}H-NMR spectra were acquired on a Bruker Ascend 400 MHz-Avance III HD NMR spectrometer (Bruker Corporation, Billerica, MA, USA) as solutions in deuterated dimethyl sulfoxide (DMSO-d_6). Chemical shifts (δ) for ^{1}H-NMR spectra are reported in parts per million (ppm) relative to the solvent residual peak at 2.50 ppm. Multiplicities of peaks are represented by s (singlet) and m (multiplet). All spectra were processed for recorded FID files with MestReNova 12.0.1 software (Mestrelab Research, Santiago de Compostela, Spain).

2.2.6. Calculation of empirical formulas of STZ, (MeO-PEG-NH_2)$_{10kDa}$ and (MeO-PEG-NH)$_{10kDa}$-STZ by elemental CHNS(O) analysis

The percentages of C, H, N, and S were recorded on dried samples of STZ, (MeO-PEG-NH_2)$_{10kDa}$ and (MeO-PEG-NH)$_{10kDa}$-STZ by using a vario MICRO cube CHNS analyzer (Elementar Analysensysteme GmbH, Langenselbold, Germany). The percentage of O was calculated by subtracting the percentages of C, H, N, and S from 100%. Sulphanilamide, the manufacturer recommended calibration standard, was run daily, prior to sample analysis and interspersed between samples, to compute the daily factor, the variation between the daily instrument response relative to the factory calibration, in order to apply the appropriate calibration factor (16.25% N, 41.81% C, 18.62% S, 4.65% H). The daily factor was also run to calculate the systematic error for analysis. Integration limits set are reported in **Table 1**. The integration limits represent the peak area of each element obtained from the elemental analysis. Empirical formulas were calculated based on the percentage of each element and the respective theoretical empirical formulas of STZ ($C_{21}H_{32}N_2O$), (MeO-PEG-NH_2)$_{10kDa}$ ($C_5H_{13}NO_2{\cdot}[C_2H_4O]_{225}$) and (MeO-PEG-NH)$_{10kDa}$-STZ ($C_{27}H_{43}N_3O_4{\cdot}[C_2H_4O]_{225}$). If integrated areas were under integration limits, the elements were under the limit of quantification (LOQ).

2.2.7. Matrix-assisted laser desorption/ionization time-of-flight/time-of-flight mass spectrometry (MALDI-TOF/TOF MS)

$(MeO\text{-}PEG\text{-}NH_2)_{10kDa}$ and $(MeO\text{-}PEG\text{-}NH)_{10kDa}$-STZ were analyzed by Ultraflex MALDI TOF/TOF instrument (Bruker Daltonics GmbH, Bremen, Germany) equipped with a nitrogen laser operating at 337 nm. The mass spectra were acquired in positive ion linear and/or reflector mode using ultrapure Sinapic acid (Sigma-Aldrich, USA) as the matrix and external calibration with Protein calibration standard I (Bruker part # 206355).

$(MeO\text{-}PEG\text{-}NH_2)_{10kDa}$: m/z 5065.0, Intens. 129.00; 5122.5, 129.00; 5174.2, 132.00; 5228.3, 146.00; 5244.7, 143.00; 5344.2, 148.00; 5354.9, 131.00; 5371.9, 133.00; 5398.0, 152.00; 5439.6, 156.00; 5463.2, 154.00; 5487.2, 141.00; 5494.0, 157.00; 5514.1, 155.00; 5526.3, 133.00; 5536.0, 153.00; 5553.0, 151.00; 5581.2, 139.00; 5589.8, 166.00; 5602.9, 154.00; 5613.8, 135.00; 5625.9, 137.00; 5667.1, 131.00; 5669.3, 129.00; 5694.5, 150.00; 5711.8, 147.00; 5751.4, 141.00; 5817.6, 138.00; 5842.1, 135.00; 5904.9, 138.00; 5922.8, 151.00; 5950.8, 148.00; 5968.9, 169.00; 5986.3, 142.00; 5999.6, 153.00; 6068.0, 134.00; 6152.9, 138.00; 6216.5, 136.00; 6337.2, 134.00; 10225.2, 139.00; 10282.5, 130.00; 10580.4, 150.00; 10674.6, 133.00; 10726.5, 135.00; 10763.7, 134.00; 10820.1, 142.00; 10843.9, 142.00; 10936.6, 134.00; 10997.3, 133.00; 11040.8, 133.00

$(MeO\text{-}PEG\text{-}NH)_{10kDa}$-STZ: m/z 5240.9, Intens. 56.00; 5462.7, 68.00; 5550.5, 58.00; 5559.4, 72.00; 5572.1, 58.00; 5598.9, 57.00; 5742.2, 60.00; 5840.9, 60.00; 5886.5, 56.00; 5970.0, 62.00; 6076.8, 59.00; 6399.6, 55.00; 10116.8, 69.00; 10128.2, 58.00; 10142.5, 56.00; 10251.0, 64.00; 10253.3, 56.00; 10268.4, 60.00; 10286.4, 57.00; 10302.2, 64.00; 10318.4, 55.00; 10337.7, 61.00; 10351.3, 66.00; 10371.6, 55.00; 10408.4, 68.00; 10429.6, 60.00; 10473.6, 69.00; 10495.5, 64.00; 10514.7, 74.00; 10530.6, 65.00; 10556.8, 56.00; 10574.5, 60.00; 10594.2, 88.00; 10619.9, 73.00; 10655.4, 60.00; 10691.0, 82.00; 10710.3, 63.00; 10778.1, 71.00; 10794.8, 67.00; 10813.8, 75.00; 10843.2, 62.00; 10856.9, 67.00; 10912.5, 63.00; 10963.2, 60.00; 11002.1, 60.00; 11059.1, 57.00; 11076.4, 67.00; 11099.1, 57.00; 11140.1, 65.00; 11303.0; 66.00

2.2.8. Cross reactivity of STZ and $(MeO\text{-}PEG\text{-}NH)_{10kDa}$-STZ toward TST by AChE competitive enzyme-linked immunosorbent assay (ELISA)

The competition between TST, STZ and $(MeO\text{-}PEG\text{-}NH)_{10kDa}$-STZ and a TST-AChE conjugate (TST tracer) for a limited amount of TST antiserum was estimated by the commercial Testosterone ELISA-Kit (Cayman Chemical, Ann Arbor, MI, USA). The ratio of the absorbance read at 412 nm of a particular sample (B) to that of the maximum TST tracer amount (B_0) bound by the antibody in the absence of free analyte was calculated in duplicate for four different concentrations (500, 125, 31.25 and 7.8125 pg/mL) of TST, STZ and $(MeO\text{-}PEG\text{-}NH)_{10kDa}$-STZ, according to the manufacturer's instructions available at the following URL: https://www.caymanchem.com/pdfs/582701.pdf (**Table 2**). Cross reactivity is calculated by comparing the mid-point (50% B/B_0) value of TST, STZ and

$(MeO\text{-}PEG\text{-}NH)_{10kDa}$-STZ to the mid-point (50% B/B_0) value of TST when each is measured in assay buffer using the following formula:

$$\%\textbf{Cross recovery} = \left[\frac{50\%\frac{B}{B_0}\textbf{ value for TST}}{50\%\frac{B}{B_0}\textbf{ value for TST, STZ and }(MeO-PEG-NH)_{10kDa}-STZ}\right] \times 100$$

Molecules that possess similar epitopes to the primary analyte of interest (TST) can compete with the TST tracer for binding to the primary antibody (monoclonal anti-rabbit IgG that has been previously attached to the well from the company in the commercial kit). Cross reactivity by considering alone TST is considered as 100%. Substances that are superior to the analyte, in displacing the tracer, result in a cross reactivity that is greater than 100%. Whereas, substances that are inferior to the primary analyte, in displacing the tracer, result in a cross reactivity that is less than 100%.

2.2.9 Cell culture and cytotoxicity of STZ, $(MeO\text{-}PEG\text{-}NH_2)_{10kDa}$ and $(MeO\text{-}PEG\text{-}NH)_{10kDa}$-STZ

Saos-2 cells were cultured as already reported elsewhere (**Cristiano et al., 2017**). Briefly, cells were seeded in T75 cell culture flasks for growing adherent cells (Thermo Fisher Scientific, Italy), containing McCoy's 5A medium supplemented with penicillin (100 UI/ml), streptomycin (100 µg/ml), amphotericin B (250 µg/ml) and FBS (10%, v/v), at 37 °C in a humidified atmosphere of 5% CO_2 (Guaire® TS Autoflow Codue Water-Jacketed Incubator). Medium was refreshed every 48 h. Cells reaching the 70% of confluence were splatted adding 2 mL of trypsin, then further amplified after being collected by centrifugation for 10 min. at 1000 RPM and RT (Eppendorf Centrifuge 58100, Eppendorf, Hamburg, Germany).

Cytotoxicity of $(MeO\text{-}PEG\text{-}NH)_{10kDa}$-STZ, compared with free STZ and $(MeO\text{-}PEG\text{-}NH_2)_{10kDa}$, was evaluated by performing the 3-(4,5-dimethylthiazol-2-yl)-2,5-diphenyltetrazolium bromide (MTT) assay for up 80 h. The percentage of viable cells was indirectly determined by MTT dye reduction. Indeed, MTT is reduced by active mitochondria in living cells (**Mosmann, 1983**). MTT assay was performed according to the modified method firstly described by Sladowski et al. in 1993 (**Sladowski et al., 1993**). Briefly, 10×10^3 Saos-2 cells/0.2 mL of McCoy's 5A supplemented medium were cultured in the 96-well plate (Thermo Fisher Scientific, Italy) for 24 h at 37 °C (**Gao et al., 2019**; **Morsi et al., 2019**). Subsequently, the culture medium was replaced with 0.2 mL of McCoy's 5A supplemented medium containing 1, 10, 25 or 50 µM STZ and/or $(MeO\text{-}PEG\text{-}NH)_{10kDa}$-STZ, which were solubilized in a minimal volume of DMSO, then in the same culture medium by fixing the number of equivalent weights of STZ. Cell culture medium (CCM), DMSO and $(MeO\text{-}PEG\text{-}NH_2)_{10kDa}$ were used as controls. After 1, 4, 20 or 80 h, 20 µL of MTT solution (5 mg of 3-(4,5-dimethylthiazol-2-yl)-2,5-diphenyltetrazolium bromide/mL of PBS) were added to each well and left under incubation for 3 h (**De Rose et al., 2016**). 200 µL of a solution of DMSO/ethanol (1:1, v/v) was

added to each well after discarding the supernatants. After a stirring of 20 min. at 230 RPM on the orbital shaker KS130 Control (IKA®-Werke GmbH & CO, Staufen imBreisgau, Germany), the absorbance (Abs) of dissolved MTT formazan crystals was read at 570 nm by using the xMark™ Microplate Absorbance Spectrophotometer (Bio-Rad, Hercules, CA, USA). The cell viability percentage was calculated by using the following equation:

$$\text{Cell viability (\%)} = (\text{AbsT}/\text{AbsC}) \times 100$$

where AbsT is the absorbance of the absorbance of cells that has undergone a treatment and AbsC is the absorbance of control (untreated) cells. Three different independent experiments were done in duplicate.

3. Results and Discussion

HPLC is a powerful analytical technique that is widely used for the measurement of PEGylated small drugs (**Cheng et al., 2012**). HPLC spectra of STZ and $(MeO\text{-}PEG\text{-}NH)_{10kDa}$-STZ conjugate are shown in Figs 1A-B, respectively. As shown in **Fig. 1B**, RP-HPLC of $(MeO\text{-}PEG\text{-}NH)_{10kDa}$-STZ conjugate (total run time of 45 min.) demonstrates the synthesis of a pure compound (purity grade ≥ 99%), thus validating the process of purification used during the synthesis of product (see **Section 2.2.2.**). Due to the physicochemical property of the attached PEG, a longer retention time for PEGylated STZ was expected, as previously reported for PEGylated peptides (**Park and Na, 2016**). In fact, STZ eluted as a single peak at about 15 min. (**Fig. 1A**, 15.0 min), whereas $(MeO\text{-}PEG\text{-}NH)_{10kDa}$-STZ conjugate postponed its elution time at about 28 min. (**Fig. 1B**, 27.6 min.).

Besides increasing water solubility, PEGylation increases stability of drugs, minimizing their cleavage and therefore increasing their half-life (**Veronese and Pasut, 2005**; **Conover et al., 2003**). In order to mimic the pH, osmolarity, and ion concentrations of the human body fluids, the stability of PEGylated STZ (1 mg/mL) was evaluated in phosphate buffer (PB) solution, buffered at pH 7.4 and 5.8, by performing quantitative RP-HPLC analyses (see **Section 2.2.3.**). PB at pH 7.4 simulates human blood and its normal pH value, which is tightly regulated between 7.35 and 7.45. On the other hand, PB at pH 5.8 is considered like fluids of acidic organelles, such as lysosomes, which have a pH value ranged between 3.5 and 6.0 (**Casey et al., 2010**). Lysosomes contain hydrolases that facilitate the decomposition of proteins, lipids, and polysaccharides. These enzymes are active in acidic conditions, requiring the organelle to maintain an optimal luminal pH between 4 and 5 (**Pillay et al., 2002**). Prolonged STZ administration provokes an increase in the activities of these liver lysosomal hydrolases (**Molano et al., 1999**), thus showing their involvement in the drug degradation. Interestingly, RP-HPLC analyses have shown a very high stability of $(MeO\text{-}PEG\text{-}NH)_{10kDa}$-STZ conjugate at both pH values throughout 80 h (**Fig. 2**). In particular, after 80 h the (MeO-PEG-

$NH)_{10kDa}$-STZ amounts found in the PB solution ranged between 69.83% (PB, pH 5.8) and 87.27% (PB, pH 7.4). Conversely, at the same time point, the amounts of STZ was ranged between 10.28% (PB, pH 5.8) and 11.67% (PB, pH 7.4) (**Fig. 2**). The solubility of STZ in the PEG conjugate increased up to approximately 260-269×10^3 times than bare STZ, as measured in mQ water (25 °C, 1 atm) (**Table 3**). These data agree with those previously obtained by Conover and co-authors, who demonstrated that different PEG_{40kDa}-Amphotericin B conjugates showed less hydrolysis following 24 h incubation in PB pH 7.4 and greater solubility in aqueous solutions than free PEG_{40kDa} and Amphotericin B, as a result of PEGylation (**Conover et al., 2003**). These data could involve the reduction of drug administration frequency, thus enhancing both compliance and life quality of patients (**Cheng et al., 2012**; **Veronese and Pasut, 2005**).

As it can be seen from ATR-FTIR spectra in **Fig. 3**, a broad and small IR signal in the range 3425-3075 cm^{-1}, belonging to the stretching frequency of a free alcohol (OH) group, can be assigned to OH group bonded to the C_{17} of STZ. As expected, this signal is not present in both $(MeO\text{-}PEG\text{-}NH_2)_{10kDa}$ and $(MeO\text{-}PEG\text{-}NH)_{10kDa}$-STZ compounds. Indeed, in $(MeO\text{-}PEG\text{-}NH_2)_{10kDa}$ there are no OH groups. In addition, the nucleophilic substitution by 4-nitrophenyl chloroformate at the OH group bonded to the C_{17} of STZ allows the synthesis of 17-(4-nitrophenyl carbonate) STZ (Product 1, **Scheme 1**). This is why the signal of any OH group is not present in the spectrum of $(MeO\text{-}PEG\text{-}NH)_{10kDa}$-STZ conjugate. All vibrational modes (3^{n-6} = 162 normal modes) of STZ, defining 60 stretching, 122 bending, and 28 torsion internal coordinates, by including redundancies (**Lemma et al., 2017**), may be found in its relative IR spectrum (**Fig. 3**). It is much more difficult to pick out individual bonds in the region to the right-hand side of the diagram from about 1875 to 625 cm^{-1} (fingerprint region). Even though these complicated series of absorptions are due to all configurations of bending vibrations within all analyzed molecules, the characteristic signal of PEG in $(MeO\text{-}PEG\text{-}NH_2)_{10kDa}$ and $(MeO\text{-}PEG\text{-}NH)_{10kDa}$-STZ compounds is present in the resulting ATR-FTIR spectra (**Dupeyrón et al., 2013**). The synthesis of $(MeO\text{-}PEG\text{-}NH)_{10kDa}$-STZ conjugate is confirmed by the stretching of carbamate CN bond falling at around 2025-1925 cm^{-1}.

The carbamate CN bond belonging to $(MeO\text{-}PEG\text{-}NH)_{10kDa}$-STZ conjugate was also confirmed by performing the ^{1}H-NMR characterization of the resulting synthetic product. Indeed, by comparing the chemical shift (δ) assignments for each proton signal belonging to STZ (see carbon numbering of STZ molecular structure reported in **Fig. 4A**) with those of $(MeO\text{-}PEG\text{-}NH)_{10kDa}$-STZ (**Fig. 4C**), they are easily recognizable: (i) the range of chemical shifts belonging to hydrogens of $(OCH_2CH_2)O$-group (**Fig. 4B-C**; backbone peak, δ = 3.0-4.0 ppm,) (**Dust et al., 1990**); (ii) the chemical shift belonging to hydrogen of -NHCO- group (**Fig. 4C**; single peak, δ = 5.574) (**Digilio et al., 2003**).

$C_{21}H_{32}N_2O$, $C_5H_{13}NO_2{\cdot}[C_2H_4O]_{225}$ and $C_{27}H_{43}N_3O_4{\cdot}[C_2H_4O]_{225}$ are the theoretical empirical formulas of STZ, $(MeO\text{-}PEG\text{-}NH_2)_{10kDa}$ and $(MeO\text{-}PEG\text{-}NH)_{10kDa}$-STZ, respectively (**Scheme 1**). According to their empirical formula, specific percentage compositions for the chemical elements N, C, H, and O are expected. As shown in the **Table 4**, the elemental CHNS(O) analysis did not confirm the percentage compositions exactly such as predicted, especially for $C_5H_{13}NO_2{\cdot}[C_2H_4O]_{225}$ and $C_{27}H_{43}N_3O_4{\cdot}[C_2H_4O]_{225}$. The results obtained fit better to $C_5H_{13}NO_2{\cdot}[C_2H_4O]_{248}$ and $C_{27}H_{43}N_3O_4{\cdot}[C_2H_4O]_{248}$, *i.e.*, for minimal formula including a greater number of C_2H_4O units. As usually it happens, the supplier could have produced a $MeO\text{-}PEG\text{-}NH_2$ with a slightly higher MW close to 11000 Da than the declared one (10 kDa, Iris Biotech GmbH, Product code: PEG1151). Nevertheless, the difference between the theoretical percentage composition and that found experimentally ($\left|\text{Diff.}\right|$) about the chemical elements N, C, H and O never exceeded 0.5. The low values of $\left|\text{Diff.}\right|$, besides confirming the predicted empirical formulas, demonstrate also that the obtained products, especially about STZ and $(MeO\text{-}PEG\text{-}NH)_{10kDa}$-STZ, maintained their structural double bonds, thus confirming their high stability. Since elemental CHNS(O) analysis is based on a combustion process, the percentage of O was calculated by subtracting to 100% the relative percentage of the chemical elements N, C, H and S. The latter chemical element was quantified in order to evaluate possible reaction impurities. It is worth noting that this very low deviation means having obtained very pure reaction products. In fact, the percentages of S never exceeded 0.09%, proving that the nitrogen and sulfur were under the limit of quantification (LOQ) of their respective calibration curves.

MWs of $(MeO\text{-}PEG\text{-}NH_2)_{10kDa}$ and $(MeO\text{-}PEG\text{-}NH)_{10kDa}$-STZ were also investigated by MALDI-TOF/TOF MS. As shown in **Fig. 5**, $(MeO\text{-}PEG\text{-}NH_2)_{10kDa}$ gives rise to a characteristic MS fragmentation, further confirmed in the MS fragmentation of $(MeO\text{-}PEG\text{-}NH)_{10kDa}$-STZ. Indeed, due to its characteristic fragmentation pattern allowing accurate and reproducible tuning, PEG is often used as an internal calibration compound in MS analyses. In the spectrum of $(MeO\text{-}PEG\text{-}NH_2)_{10kDa}$ (**Fig. 5A**), the heaviest ion, which is the product ion m/z 11040.8, is likely to be the molecular ion M^+. Even though the difference in MW found here compared to what declared by the supplier is not to be considered significant for this type of polymers (ΔMW = 1040.8 Da, +10.4% than declared by supplier), again, this value did not match its nominal MW (10 kDa). Conversely, it almost fits perfectly with a compound having a minimal formula $C_5H_{13}NO_2{\cdot}[C_2H_4O]_{248}$, therefore a MW of 11044.2 Da (ΔMW = 3.4 Da). M^+ of $(MeO\text{-}PEG\text{-}NH)_{10kDa}$-STZ is found at m/z 11303.0 instead at m/z 10385.5. Once again, this value of m/z found in the spectrum fits perfectly with a value of m/z 11398.7, *i.e.*, for a M^+ ensuing from the compound $C_5H_{13}NO_2{\cdot}[C_2H_4O]_{248}$. Peaks found at lower m/z can be assigned to product ions resulting from fragmentation of $(MeO\text{-}PEG\text{-}NH_2)_{10kDa}$, either alone

or if conjugated with STZ to form (MeO-PEG-NH)$_{10kDa}$-STZ (see **Section 2.2.7.**). This data fits with the finding of Onigbinde *et al*. (2013), who found that methane positive-ion mode chemical ionization of PEGs gives rise to spectra in which the peaks consist mostly of MH^+, $(C_2H_4O)_nH^+$, $(H(OC_2H_4)_nOH)H_2^+$, and $CH_3(OC_2H_4)_n^+$ ions and small amount of $C_2H_5OC_2H_4^+$ ions (**Onigbinde et al., 2013**).

Once the chemical nature of the compound (MeO-PEG-NH)$_{10kDa}$-STZ has been stated, its competitiveness against TST was evaluated. In particular, cross reactivity of different concentrations (500, 125, 31.25 and 7.8125 pg/mL) of TST, STZ or (MeO-PEG-NH)$_{10kDa}$-STZ against the same concentrations of TST was evaluated by performing AChE competitive ELISA (see **Section 2.2.8.**). STZ or (MeO-PEG-NH)$_{10kDa}$-STZ were less able than TST to displace the AChE-linked TST bound to TST antiserum (**Fig. 6**). STZ has low affinity for binding the AR too. However, it strongly activates AR-mediated signaling (**Feldkoren, and Andersson, 2005**). Surprisingly, cross reactivity of STZ or (MeO-PEG-NH)$_{10kDa}$-STZ against TST increased with decreasing concentrations, (MeO-PEG-NH)$_{10kDa}$-STZ more than STZ ($p<0.05$). Differences in physicochemical properties (*e.g.*, water solubility, specificity of immunoassay for the principal ligand) between TST and STZ, either alone or as (MeO-PEG-NH)$_{10kDa}$-STZ, could explain this phenomenon (**Miller and Valdes, 1991**). Nevertheless, the fact that (MeO-PEG-NH)$_{10kDa}$-STZ competes against biological TST at lower concentrations, with a cross reactivity close to 100%, makes it very useful as a drug.

Fig. 7A-D shows the cytotoxicity time-courses (for up 80 h) of increasing concentrations (1, 10, 25 or 50 µM) of STZ and/or (MeO-PEG-NH)$_{10kDa}$-STZ that have been evaluated using the MTT assay on human osteosarcoma Saos-2 cells, which express AR and are responsive to STZ (**Ghiacci et al., 2018**; **Orwoll et al., 1991**). STZ decreased the cell viability of both glial and neuronal primary cortical cells up to 24 h of treatment and in the range of concentrations from 10 to 100 µM. Intermediate concentrations of STZ (10 and 30 µM), administered every 24 h for three consecutive days, resulted still nontoxic to cells, while higher concentrations (100 µM) reduced cell viability by about 50% (**Zelleroth et al., 2019**). Conversely, STZ affects the cell viability of Saos-2 cells, by inducing a cell loss of 17% already after 4 h of treatment, at a concentration 1 µM (STZ *vs.* CCM, $p<0.05$; **Fig. 7A**). This cell loss reached 96% after 80 h of treatment, at a concentration 50 µM (STZ *vs.* CCM, $p<0.05$; **Fig. 7D**). Interestingly, high values of cell vitality were obtained upon treatment with (MeO-PEG-NH)$_{10kDa}$-STZ, due to the presence of (MeO-PEG-NH$_2$)$_{10kDa}$ (**Fig. 7A-D**). In fact, compared to STZ-treated cells, cells treated with (MeO-PEG-NH)$_{10kDa}$-STZ showed cell viability values in the range from +3% (1 µM at 20 h, $p<0.05$; **Fig. 7A**) to +41% (50 µM at 4 h, $p<0.05$; **Fig. 7D**). PEGs have generally been reported to be nontoxic to cells (**Kaul et al., 2002**). Indeed, (MeO-PEG-NH$_2$)$_{10kDa}$, when compared to the alone CCM, showed the least toxic tested for cells if compared to other

formulations, thus decreasing cell viability by 39% after 80 h of treatment at a concentration of 50 μM ($p<0.05$; **Fig. 7D**). This lack of toxicity may depend on that generally PEGs do not bind to the proteins of cells (**Lee et al., 1995**). Furthermore, PEGylation of inorganic nanoparticles, like nanorods, lack significantly their cytotoxicity *in vitro* on human endothelial cells (**Li et al., 2019**). To demonstrate that it was the STZ and not the $(MeO\text{-}PEG\text{-}NH_2)_{10kDa}$ to be cytotoxic, intermediate cell viability values between STZ-treated and $(MeO\text{-}PEG\text{-}NH)_{10kDa}$-STZ-treated cells, closer to the first ones, were observed when the Saos-2 cells underwent the treatment $(MeO\text{-}PEG\text{-}NH)_{10kDa}$-STZ + STZ (**Fig. 7A-D**). DMSO, which has been used at the minimum volume to dissolve STZ and have the stock solution for *in vitro* experiments (see **Section 2.2.9**), was nontoxic to cells. DMSO was toxic for Saos-2 cells after 20 h of treatment at a concentration of 50 μM, when a decrease of 38% in cell viability was obtained compared to cells treated with CCM alone ($p<0.05$; **Fig. 7D**).

4. Conclusions

As confirmed by RP-HPLC, ATR-FTIR, ^{1}H-NMR, elemental CHNS(O) and MALDI-TOF/TOF MS analyses, a $(MeO\text{-}PEG\text{-}NH)_{10kDa}$-STZ conjugate was synthesized with a high degree of purity. PEGylation increased stability and water solubility of STZ, therefore its bioavailability and efficacy (**Cheng et al., 2012**; **Veronese and Pasut, 2005**; **Conover et al., 2003**). RP-HPLC analysis has shown a very high stability of $(MeO\text{-}PEG\text{-}NH)_{10kDa}$-STZ conjugate in PB, buffered either at pH 5.8 and at 7.4, for up 80 h at 37 °C. In addition, higher drug bioavailability and efficacy can decrease the frequency of administration and thus increasing the compliance and life quality of patients (**Cheng et al., 2012**; **Veronese and Pasut, 2005**). AChE competitive ELISA showed that this compound competes against biological TST especially at lower concentrations. Saos-2 cell viability data demonstrated that PEGylation opposed the cytotoxicity of STZ alone, with $(MeO\text{-}PEG\text{-}NH)_{10kDa}$-STZ inducing higher cell viability values than STZ, especially at higher drug concentrations. Conversely, resulting data showed that $(MeO\text{-}PEG\text{-}NH)_{10kDa}$-STZ could be taken into consideration as a promising and reliable drug to be used in clinical conditions requiring TST.

Conflict of interest

The author declares no competing financial interest.

Acknowledgements

This manuscript was partially supported by FAR 2017, MIUR grant, University of Chieti - Pescara "G. d'Annunzio", Chieti, Italy, and FFARB 2017, Fondo per il Finanziamento delle Attività di Base di Ricerca, Prof. Christian Celia and Prof. Felisa Ciluzo, MIUR grant. Prof. H. A. Santos

acknowledges financial support from the HiLIFE Research Funds and the Sigrid Juselius Foundation (Grant No. 4704580).

References

Akiyama, Y., Otsuka, H., Nagasaki, Y., Kato, M., Kataoka, K., 2000. Selective synthesis of heterobifunctional poly(ethylene glycol) derivatives containing both mercapto and acetal terminals. Bioconjug. Chem. 11, 947-950. https://doi.org/10.1021/bc000034w.

Azri, A., Giamarchi, P., Grohens, Y., Olier, R., Privat, M., 2012. Polyethylene glycol aggregates in water formed through hydrophobic helical structures. J. Colloid. Interface Sci. 379, 14-19. https://doi.org/10.1016/j.jcis.2012.04.025.

Bienenfeld, A., Azarchi, S., Lo Sicco, K., Marchbein, S., Shapiro, J., Nagler, A.R., 2018. Androgens in women: androgen mediated skin disease and patient evaluation (Part I). J. Am. Acad. Dermatol. 80, 1497-1506. https://doi.org/10.1016/j.jaad.2018.08.062.

Cheng, T.L., Chuang, K.H., Chen, B.M., Roffler, S.R., 2012. Analytical measurement of PEGylated molecules. Bioconjug. Chem. 23, 881-899. https://doi.org/10.1021/bc200478w.

Conover, C.D., Zhao, H., Longley, C.B., Shum, K.L., Greenwald, R.B., 2003. Utility of poly(ethylene glycol) conjugation to create prodrugs of amphotericin B. Bioconjug. Chem. 14, 661-666. https://doi.org/10.1021/bc0256594.

Cristiano, M.C., Cosco, D., Celia, C., Tudose, A., Mare, R., Paolino, D., Fresta, M., 2017. Anticancer activity of all-trans retinoic acid-loaded liposomes on human thyroid carcinoma cells. Colloids Surf. B Biointerfaces 150, 408-416. https:dor.org/10.1016/j.colsurfb.2016.10.052.

Davis, S.R., Wahlin-Jacobsen, S., 2015. Testosterone in women-the clinical significance. Lancet Diabetes Endocrinol 3, 980-992. https://doi.org/10.1016/S2213-8587(15)00284-3.

De Rose, R.F., Cristiano, M.C., Celano, M., Maggisano, V., Vero, A., Lombardo, G.E., Di Francesco, M., Paolino, D., Russo, D., Cosco, D., 2016. PDE5 inhibitors-loaded nanovesicles: physico-chemical properties and in vitro antiproliferative activity. Nanomaterials (Basel) 6, pii: E92. https://doi.org/10.3390/nano6050092.

Digilio, G., Barbero, L., Bracco, C., Corpillo, D., Esposito, P., Piquet, G., Traversa, S., Aime, S., 2003. NMR structure of two novel polyethylene glycol conjugates of the human growth hormone-releasing factor, hGRF(1-29)-NH2. J. Am. Chem. Soc. 125, 3458-3470. https://doi.org/10.1021/ja021264j.

Donner, D.G., Elliott, G.E., Beck, B.R., Forwood, M.R., Du Toit, E.F., 2016. The effects of visceral obesity and androgens on bone: trenbolone protects against loss of femoral bone mineral density

and structural strength in viscerally obese and testosterone-deficient male rats. Osteoporos. Int. 27, 1073-1082. https://doi.org/10.1007/s00198-015-3345-1.

Dupeyrón, D., Kawakami, M., Ferreira, A.M., Cáceres-Vélez, P.R., Rieumont, J., Azevedo, R.B., Carvalho, J.C., 2013. Design of indomethacin-loaded nanoparticles: effect of polymer matrix and surfactant. Int. J. Nanomedicine 8, 3467-6477. https://doi.org/10.2147/IJN.S47621.

Dust, J.M., Fang, Z.H., Harris, J.M., 1990. Proton NMR characterization of poly(ethylene glycols) and derivatives. Macromolecules 23, 3742-3746. https://doi.org/10.1021/ma00218a005.

El Osta, R., Almont, T., Diligent, C., Hubert, N., Eschwège, P., Hubert, J., 2016. Anabolic steroids abuse and male infertility. Basic Clin. Androl. 26, 2. https://doi.org/10.1186/s12610-016-0029-4.

Fasinu, P., Pillay, V., Ndesendo, V.M., du Toit, L.C., Choonara, Y.E, 2011. Diverse approaches for the enhancement of oral drug bioavailability. Biopharm. Drug Dispos. 32, 185-209. https://doi.org/10.1002/bdd.750.

Feldkoren, B.I., Andersson, S., 2005. Anabolic-androgenic steroid interaction with rat androgen receptor in vivo and in vitro: a comparative study. J. Steroid. Biochem. Mol. Biol. 94, 481-487. https://doi.org/10.1016/j.jsbmb.2004.12.036.

Gao, K., Su, Z., Liu, H., Liu, Y., 2019. Anti-proliferation and anti-metastatic effects of sevoflurane on human osteosarcoma U2OS and Saos-2 cells. Exp. Mol. Pathol. 108, 121-130. https://doi.org/10.1016/j.yexmp.2019.04.005.

Ghiacci, G., Graiani, G., Cacchioli, A., Galli, C., Lumetti, S., Ravanetti, F., Elviri, L., Manfredi, E., Macaluso, G.M., Sala, R., 2017. Stanozolol-soaked grafts enhance new bone formation in rat calvarial critical-size defects. Biomed. Mater. 12, 045016. https://doi.org/10.1088/1748-605X/aa71bc.

Ghiacci, G., Lumetti, S., Manfredi, E., Mori, D., Macaluso, G.M., Sala, R., 2018. Stanozolol promotes osteogenic gene expression and apposition of bone mineral in vitro. J. Appl. Oral Sci. 27, e20180014. https://doi.org/10.1590/1678-7757-2018-0014.

Guimarães, A.P.F.G.M., Butezloff, M.M., Zamarioli, A., Issa, J.P.M., Volpon, J.B., 2017. Nandrolone decanoate appears to increase bone callus formation in young adult rats after a complete femoral fracture. Acta Cir. Bras. 32, 924-934. https://doi.org/10.1590/s0102-865020170110000004.

Harris, J.M., Chess, R.B., 2003. Effects of PEGylation on pharmaceuticals. Nat. Rev. Drug Discov. 2, 214-221. https://doi.org/10.1038/nrd1033.

JECFA, 1980. Polyethylene glycols, in: Toxicological evaluation of certain food additives, 23rd Joint FAO/WHO Expert Committee on Food Additives (JECFA) session, Apr. 2-11, 1979, Geneva,

WHO Food Additives Series No. 14, pp. 76-83. http://www.inchem.org/documents/jecfa/jecmono/v14je01.htm.

Kaul, G., Amiji, M., 2002. Long-circulating poly(ethylene glycol)-modified gelatin nanoparticles for intracellular delivery. Pharm. Res. 7, 1061-1067. https://doi.org/10.1023/a:1016486910719.

Lee, J. H., Lee, H.B., Andrade, J. D., 1995. Blood compatibility of polyethylene oxide surfaces. Prog. Polym. Sci. 20, 1043-1079. https://doi.org/10.1016/0079-6700(95)00011-4.

Lemma, T., de Barros Souza, F., Tellez Soto, C.A., Martin, A.A., 2017. An FT-Raman, FT-IR, and quantum chemical investigation of stanozolol and oxandrolone. Biosensors (Basel) 8, 2. https://doi.org/10.3390/bios8010002.

Li, X., Tang, Y., Chen, C., Qiu, D., Cao, Y. 2019. PEGylated gold nanorods are not cytotoxic to human endothelial cells but affect kruppel-like factor signaling pathway. Toxicol. Appl. Pharmacol. 382, 114758. https://doi/10.1016/j.taap.2019.114758.

Liao, J.M., Wu, T., Li, Q.N., Hu, B., Huang, L.F., Li, Z.H., Yuan, L., Zhong, S.Z., 2003. Effects of stanozolol on bone mineral density and bone biomechanical properties of osteoporotic rats. Di Yi Jun Yi Da Xue Xue Bao 23, 1117-1120. https://www.ncbi.nlm.nih.gov/pubmed/14625163.

Miah, S., Tharakan, T., Gallagher, K.A., Shah, T.T., Winkler, M., Jayasena, C.N., Ahmed, H.U., Minhas, S., 2019. The effects of testosterone replacement therapy on the prostate: a clinical perspective. F1000Res. 8, F1000 Faculty Rev-217. https://doi.org/10.12688/f1000research.16497.1.

Miller, J.J., Valdes, R. Jr., 1991. Approaches to minimizing interference by cross-reacting molecules in immunoassays. Clin. Chem. 37, 144-153. http://clinchem.aaccjnls.org/content/37/2/144.long.

Molano, F., Saborido, A., Delgado, J., Morán, M., Megías, A., 1999. Rat liver lysosomal and mitochondrial activities are modified by anabolic-androgenic steroids. Med. Sci. Sports Exerc. 31, 243-250. https://journals.lww.com/acsm-msse/Fulltext/1999/02000/Rat_liver_lysosomal_and_mitochondrial_activities.7.aspx.

Morsi, N.M., Nabil Shamma, R., Osama Eladawy, N., Abdelkhalek, A.A., 2019. Bioactive injectable triple acting thermosensitive hydrogel enriched with nano-hydroxyapatite for bone regeneration: in-vitro characterization, Saos-2 cell line cell viability and osteogenic markers evaluation. Drug Dev. Ind. Pharm. 45, 787-804. https://doi.org/10.1080/03639045.2019.1572184.

Mosmann, T., 1983. Rapid colorimetric assay for cellular growth and survival: application to proliferation and cytotoxicity assays. J. Immunol. Methods 65, 55-63. https://doi.org/10.1016/0022-1759(83)90303-4.

National Center for Biotechnology Information - PubChem Database, 2019. Stanozolol. https://pubchem.ncbi.nlm.nih.gov/compound/Stanozolol (accessed 8 Aug 2019).

Onigbinde, A.O., Munson, B., Amos-Tautua, B.M.W., 2013. Gas chromatography/chemical ionization of oligomeric polyethylene glycol mono alkyl ethers. Res. J. Chem. Sci. 3, 4-9. http://www.isca.in/rjcs/Archives/v3/i2/1.ISCA-RJCS-2012-197.pdf.

Orwoll, E.S., Stribrska, L., Ramsey, E.E., Keenan, E.J., 1991. Androgen receptors in osteoblast-like cell lines. Calcif. Tissue Int. 49, 183-187. https://doi.org/10.1007/bf02556115.

Park, E.J., Na, D.H., 2016. Characterization of the reversed-phase chromatographic behavior of PEGylated peptides based on the poly(ethylene glycol) dispersity. Analytical Chemistry 88, 10848-10853. https://doi.org/10.1021/acs.analchem.6b03577.

Pillay, C.S., Elliott, E., Dennison, C., 2002. Endolysosomal proteolysis and its regulation. Biochem. J. 363, 417-429. https://doi.org/10.1042/0264-6021:3630417.

Polik, W.F., Burchard, W., 1983. Static light scattering from aqueous poly(ethylene oxide) solutions in the temperature range 20-90°C. Macromolecules 16, 978-982. https://doi.org/10.1021/ma00240a030.

Rastrelli, G., Corona, G., Maggi, M., 2018. Testosterone and sexual function in men. Maturitas 112, 46-52. https://doi.org/10.1016/j.maturitas.2018.04.004.

Rastrelli, G., Guaraldi, F., Reismann, Y., Sforza, A., Isidori, A.M., Maggi, M., Corona, G., 2019. Testosterone replacement therapy for sexual symptoms. Sex. Med. Rev. pii, S2050-0521(18)30131-8. https://doi.org/10.1016/j.sxmr.2018.11.005.

Razzazan, A., Atyabi, F., Kazemi, B., Dinarvand, R., 2016. Influence of PEG molecular weight on the drug release and in vitro cytotoxicity of single-walled carbon nanotubes-PEG-gemcitabine conjugates. Curr. Drug Deliv. 13, 1313-1324. https://doi.org/10.2174/1567201813666160111123947.

Shin, Y.S., Park, J.K., 2019. The optimal indication for testosterone replacement therapy in late onset hypogonadism. J. Clin. Med. 8, 209. https://doi.org/10.3390/jcm8020209.

Sladowski, D., Steer, S.J., Clothier, R.H., Balls, M., 1993. An improved MTT assay. J. Immunol. Methods 157, 203–207. https://doi.org/10.1016/0022-1759(93)90088-o.

Snyder, S.L., Sobocinski, P.Z., 1975. An improved 2,4,6-trinitrobenzenesulfonic acid method for the determination of amines. Anal. Biochem. 64, 284-288.

Spadari, A., Romagnoli, N., Predieri, P.G., Borghetti, P., Cantoni, A.M., Corradi, A., 2013. Effects of intraarticular treatment with stanozolol on synovial membrane and cartilage in an ovine model of osteoarthritis. Res. Vet. Sci. 94, 379-387. https://doi.org/10.1016/j.rvsc.2012.11.020.

Veronese, F.M., Pasut, G., 2005. PEGylation, successful approach to drug delivery. Drug Discov. Today 10, 1451-1458. https://doi.org/10.1016/S1359-6446(05)03575-0.

Webster, R., Elliott, V., Park, B.K., Walker, D., Hankin, M., Taupin, P., 2009. PEG and PEG conjugates toxicity: towards an understanding of the toxicity of PEG and its relevance to PEGylated biologicals, in: Veronese, F. M. (Ed.), PEGylated protein drugs: basic science and clinical applications, milestones in drug therapy. Birkhäuser Verlag, Basel, pp. 127-146. https://doi.org/10.1007/978-3-7643-8679-5_8.

Zelleroth, S., Nylander, E., Nyberg, F., Grönbladh, A., Hallberg, M., 2019. Toxic impact of anabolic androgenic steroids in primary rat cortical cell cultures. Neuroscience 397, 172-183. https://doi.org/10.1016/j.neuroscience.2018.11.035.

Graphical Abstract caption

Stanozolol (STZ) conjugated with α-methoxy-ω-amino polyethylene glycol with nominal molecular weight (MW) of 10,000 Da, $(MeO\text{-}PEG\text{-}NH)_{10kDa}$-STZ, was synthesized to maintain the native therapeutic activity of drugs and have a water soluble and stable compound, showing the same therapeutic property of STZ. The resulting PEGylated STZ presents a promising and reliable drug to treat testosterone deficiencies.

Scheme captions

Synthesis of $(MeO\text{-}PEG\text{-}NH)_{10kDa}$-STZ conjugate. Product 1 = 17-(4-nitrophenyl carbonate) STZ; Product 2 = $(MeO\text{-}PEG\text{-}NH)_{10kDa}$-STZ; TEA = triethylamine.

Figure captions

Figure 1. Representative RP-HPLC chromatograms of STZ (A) and $(MeO\text{-}PEG\text{-}NH)_{10kDa}$-STZ (B) compounds (100 µg/mL, wavelength of UV/VIS HPLC detector set at 230 nm), by plotting the absorbance (in arbitrary units, AU) *vs*. elution time (in min.).

Figure 2. Stability of STZ, $(MeO\text{-}PEG\text{-}NH_2)_{10kDa}$ and $(MeO\text{-}PEG\text{-}NH)_{10kDa}$-STZ conjugate in PB solution, buffered at pH 5.8 and 7.4, for up 80 h at 37 °C. For each time point, the amount of intact compound that remained in solution was determined by performing quantitative RP-HPLC analysis (wavelength of UV/VIS HPLC detector set at 230 nm). Data represent the mean (± SE) of two independent experiments. * = significant value *vs.* the value reported at the time point 0 h ($p<0.05$); × = significant value with respect to the same compound in PB solution buffered at pH 5.8 ($p<0.05$).

Figure 3. Representative ATR-FTIR spectra (4000-625 cm^{-1}) of STZ (spectrum in black), $(MeO\text{-}PEG\text{-}NH_2)_{10kDa}$ (spectrum in red) and $(MeO\text{-}PEG\text{-}NH)_{10kDa}$-STZ (spectrum in green) compounds. Grey band on left side indicates the absorption range associated with alcohol bond (OH) stretching, whereas grey band on right side indicates that of carbamate bond (CN) stretching.

Figure 4. Representative ^{1}H-NMR spectra of STZ (A), $(MeO\text{-}PEG\text{-}NH_2)_{10kDa}$ (B) and $(MeO\text{-}PEG\text{-}NH)_{10kDa}$-STZ (B) compounds (for detailed information on the analysis see **Section 2.2.5.**).

Figure 5. Representative positive-ion MALDI-TOF/TOF MS spectra of $(MeO\text{-}PEG\text{-}NH_2)_{10kDa}$ (A) and $(MeO\text{-}PEG\text{-}NH)_{10kDa}$-STZ (B) compounds in the m/z range 5000-19000 (for detailed information on the analysis see **Section 2.2.7.**)

Figure 6. Cross reactivity (%) of different concentrations of TST, STZ and $(MeO\text{-}PEG\text{-}NH)_{10kDa}$-STZ toward TST (primary analyte of interest) calculated by comparing the mid-point (50%) B/B_0 value of TST, STZ or $(MeO\text{-}PEG\text{-}NH)_{10kDa}$-STZ to the mid-point (50%) B/B_0 value of TST when each was measured at 412 nm (see **Section 2.2.8.**). For each concentration point, the cross reactivity

by considering alone TST was considered as 100%. Data represent the mean (± SE) of two independent experiments. * = significant value *vs.* TST ($p<0.05$); × = significant value *vs.* (MeO-PEG-NH)$_{10kDa}$-STZ ($p<0.05$).

Figure 7. Cytotoxicity of 1 µM (A), 10 µM (B), 25 µM (C) and 50 µM (D) STZ and/or (MeO-PEG-NH)$_{10kDa}$-STZ evaluated for up 80 h by performing the MTT assay on human osteosarcoma Saos-2 cells. Cell culture medium (CCM), dimethyl sulfoxide (DMSO) and (MeO-PEG-NH$_2$)$_{10kDa}$ were used as controls. Data represent the mean (± SE) of three independent experiments as duplicate. * = significant value *vs.* CCM ($p<0.05$); × = significant value *vs.* (MeO-PEG-NH$_2$)$_{10kDa}$ ($p<0.05$); ○ = significant value *vs.* STZ ($p<0.05$).

Table captions

Table 1. Integration limits set to perform elemental CHNS(O) analysis.

Table 2. %B/B$_0$ values of TST, STZ and (MeO-PEG-NH)$_{10kDa}$-STZ as found by performing AChE competitive ELISA.

Table 3. Solubility of STZ, (MeO-PEG-NH$_2$)$_{10kDa}$ and (MeO-PEG-NH)$_{10kDa}$-STZ in milliQ water (25 °C, 1 atm).

Table 4. Elemental CHNS(O) analysis of STZ, (MeO-PEG-NH$_2$)$_{10kDa}$ and (MeO-PEG-NH)$_{10kDa}$-STZ compounds.

Element	Min	Max
N	314	29766
C	649	54507
H	22	19023
S	109	10843

Table 1

Integration limits set to perform elemental CHNS(O) analysis.

Table 2. %B/B_0 values of TST, STZ and $(MeO\text{-}PEG\text{-}NH)_{10kDa}$-STZ as found by performing AChE competitive ELISA.

Conc.(pg/mL)	**TST**				**STZ**				**(MeO-PEG-NH)$_{10kDa}$-STZ**			
			Mean	**SE**			**Mean**	**SE**			**Mean**	**SE**
500	52.1236	60.4196	**56.2716**	**4.1480**	135.7883	137.0541	**136.4212**	**0.6329**	113.0035	104.1427	**108.5731**	**4.4304**
125	61.0025	63.0481	**62.0253**	**1.0228**	134.4074	110.5944	**122.5009**	**11.9065**	106.6743	97.8136	**102.2440**	**4.4304**
31.25	61.2300	75.2487	**68.2394**	**7.0093**	126.1220	120.0230	**123.0725**	**3.0495**	86.9965	83.0840	**85.0403**	**1.9563**

SE = Standard Error.

Table 3. Solubility of STZ, $(MeO\text{-}PEG\text{-}NH_2)_{10kDa}$ and $(MeO\text{-}PEG\text{-}NH)_{10kDa}$-STZ in milliQ water (25 °C, 1 atm).

	STZ	**$(MeO\text{-}PEG\text{-}NH_2)_{10kDa}$**	**$(MeO\text{-}PEG\text{-}NH)_{10kDa}$-STZ**
Solubility (g/L)	0.00170 ± 0.00029	501.00022 ± 0.99970	449.20231 ± 0.00703
Difference in solubility with respect to that of STZ (Folds $\times 10^3$)	-	289-301	260-269

Data represent the mean (± SE) of two independent experiments.

Table 4

Compound	Run	Weight (mg)	N Area	C Area	H Area	S Area	N %	C %	H %	S %	N Factor	C Factor	H Factor	S Factor
STZ	#1	1.7440	5542	34516	13208	33	8.5500	76.1200	9.2390	0.1840	0.9737	0.9974	0.9822	1.0078
	#2	1.7760	5394	35565	13282	0	8.2600	76.6600	9.5190	0.0000	0.9838	0.9927	1.0249	1.0060
	Mean	**1.7600**	**5468**	**35040.5**	**13245**	**16.5**	**8.4050**	**76.3900**	**9.3790**	**0.0920**	**0.9788**	**0.9951**	**1.0036**	**1.0069**
	SE	**0.0160**	**74**	**524.5**	**37**	**16.5**	**0.1450**	**0.2700**	**0.1400**	**0.0920**	**0.0051**	**0.0023**	**0.0214**	**0.0009**
(MeO-PEG-NH_2)$_{10kDa}$	#1	1.7270	91	24685	11398	0	0.1600	54.7300	8.4200	0.0000	0.9838	0.9927	1.0249	1.0060
	#2	1.7560	0	25048	12118	0	0.0000	54.6100	8.7950	0.0000	0.9838	0.9927	1.0249	1.0060
	Mean	**1.7415**	**45.5**	**24.866.5**	**11.758**	**0**	**0.0800**	**54.6700**	**8.6075**	**0.0000**	**0.9838**	**0.9927**	**1.0249**	**1.0060**
	SE	**0.0145**	**45.5**	**181.5**	**360**	**0**	**0.0800**	**0.0600**	**0.1875**	**0.0000**	**0.0000**	**0.0000**	**0.0000**	**0.0000**
(MeO-PEG-NH)$_{10kDa}$-STZ	#1	1.7890	180	25584	12820	7	0.3200	55.0700	8.624	0.0410	0.9915	0.9985	0.9686	1.0931
	#2	1.7370	89	24792	11998	8	0.1600	54.6500	8.804	0.0450	0.9838	0.9927	1.0249	1.0060
	Mean	**1.7630**	**134.5**	**25188**	**12409**	**7.5**	**0.2400**	**54.8600**	**8.7140**	**0.0430**	**0.9877**	**0.9956**	**0.9968**	**1.0496**
	SE	**0.0260**	**45.5**	**396**	**411**	**0.5**	**0.0800**	**0.2100**	**0.0900**	**0.0020**	**0.0039**	**0.0029**	**0.0281**	**0.0436**

Elemental CHNS(O) analysis of STZ, (MeO-PEG-NH_2)$_{10kDa}$ and (MeO-PEG-NH)$_{10kDa}$-STZ compounds.

Compound	Minimal formula	Composition											
		N %		C %		H %		O %					
		Theoretical	Found	|Diff.|	Theoretical	Found	|Diff.|	Theoretical	Found	|Diff.|	Theoretical	Found	|Diff.|
STZ	$C_{21}H_{32}N_2O$	8.53	Up to 8.55	0.02	76.78	Up to 76.66	0.12	9.82	Up to 9.52	0.30	4.87	Down to 5.09	0.22
(MeO-PEG-NH_2)$_{10kDa}$	$C_5H_{13}NO_2{\cdot}[C_2H_4O]_{225}$	0.14	Up to 0.16	0.02	54.48	Down to 54.61	0.13	9.17	Up to 8.80	0.17	36.21	Down to 36.32	0.11
(MeO-PEG-NH_2)$_{11kDa}$	$C_5H_{13}NO_2{\cdot}[C_2H_4O]_{248}$	0.13	Up to 0.16	0.03	54.48	Down to 54.61	0.13	9.17	Up to 8.80	0.37	36.22	Down to 36.32	0.10

(MeO-PEG-NH)$_{10k\ Da}$-STZ	$C_{27}H_{43}N_3O_4 \cdot [C_2H_4O]_{225}$	0.40	Up to 0.32	0.08	55.17	Up to 54.73	0.44	9.15	Up to 8.80	0.35	35.28	Down to 35.76	0.48
(MeO-PEG-NH)$_{11k\ Da}$-STZ	$C_5H_{13}NO_2 \cdot [C_2H_4O]_{248}$	0.38	Up to 0.37	0.01	55.13	Up to 55.11	0.03	9.15	Up to 8.80	0.35	35.37	Down to 35.76	0.38

Data represent the mean (± SE) of two independent experiments. | Diff. | = difference between the theoretical percentage composition and that found experimentally.

Declaration of interests

☒ The authors declare that they have no known competing financial interests or personal relationships that could have appeared to influence the work reported in this paper.

☐The authors declare the following financial interests/personal relationships which may be considered as potential competing interests:

Scheme 1

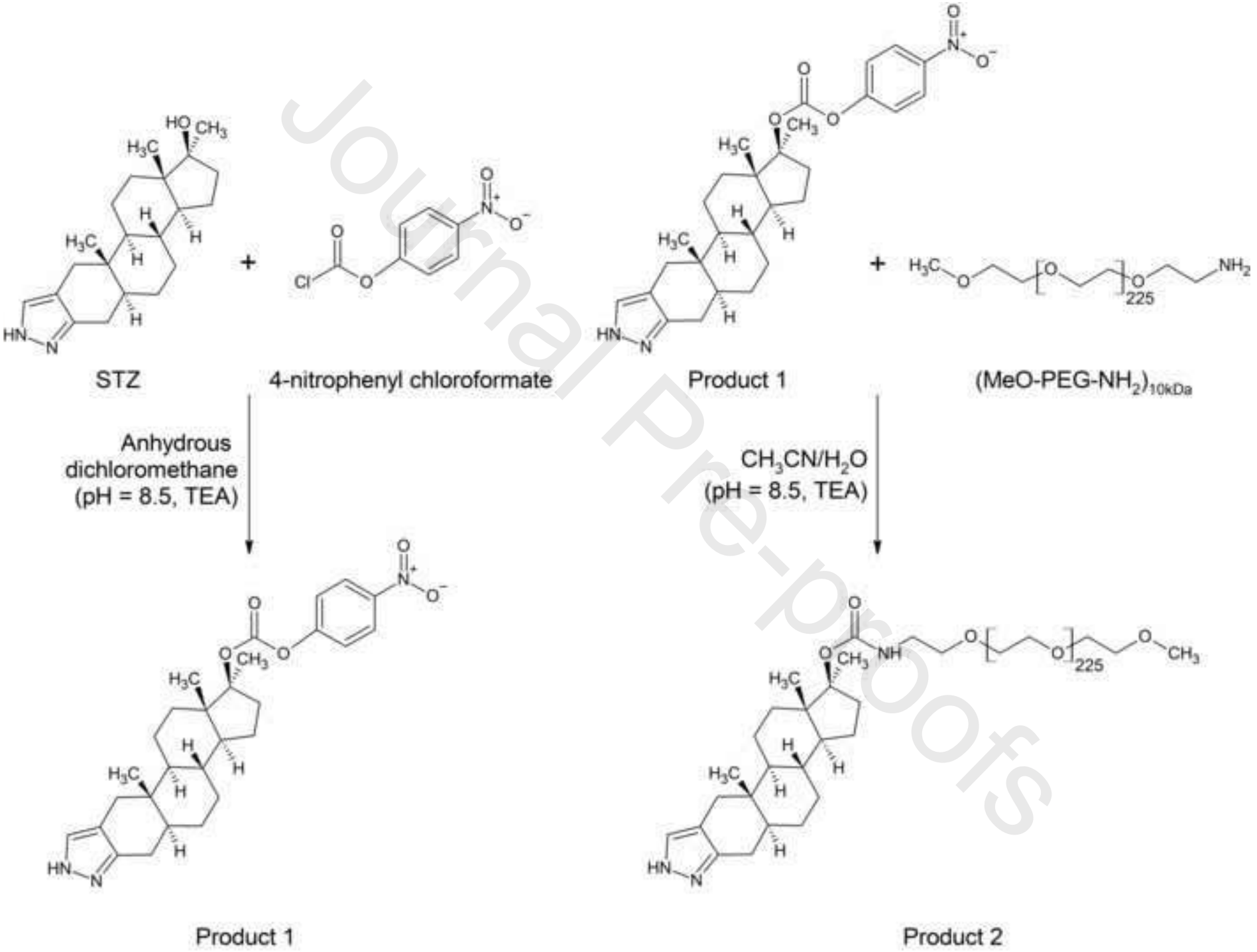

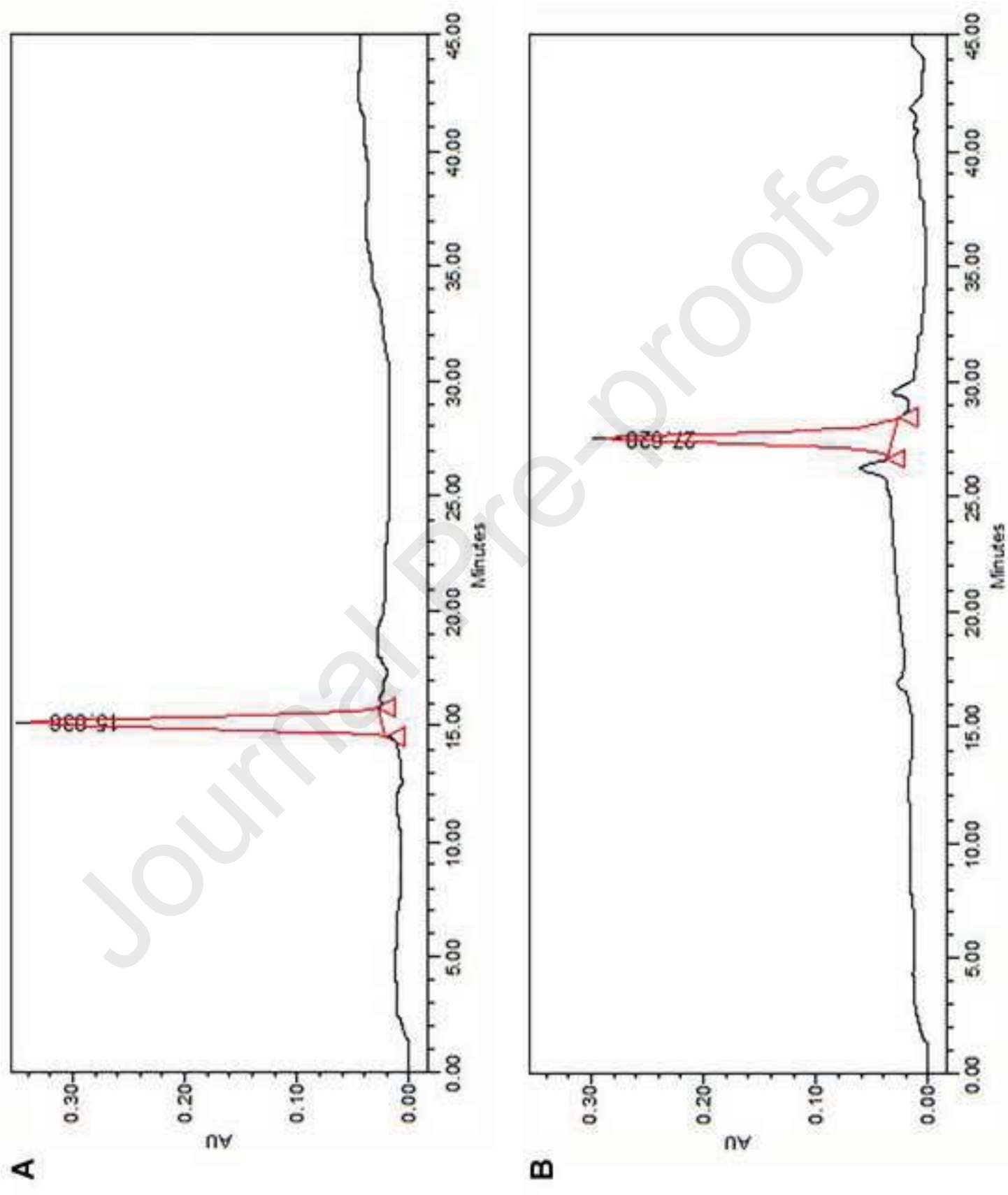

Figure 1

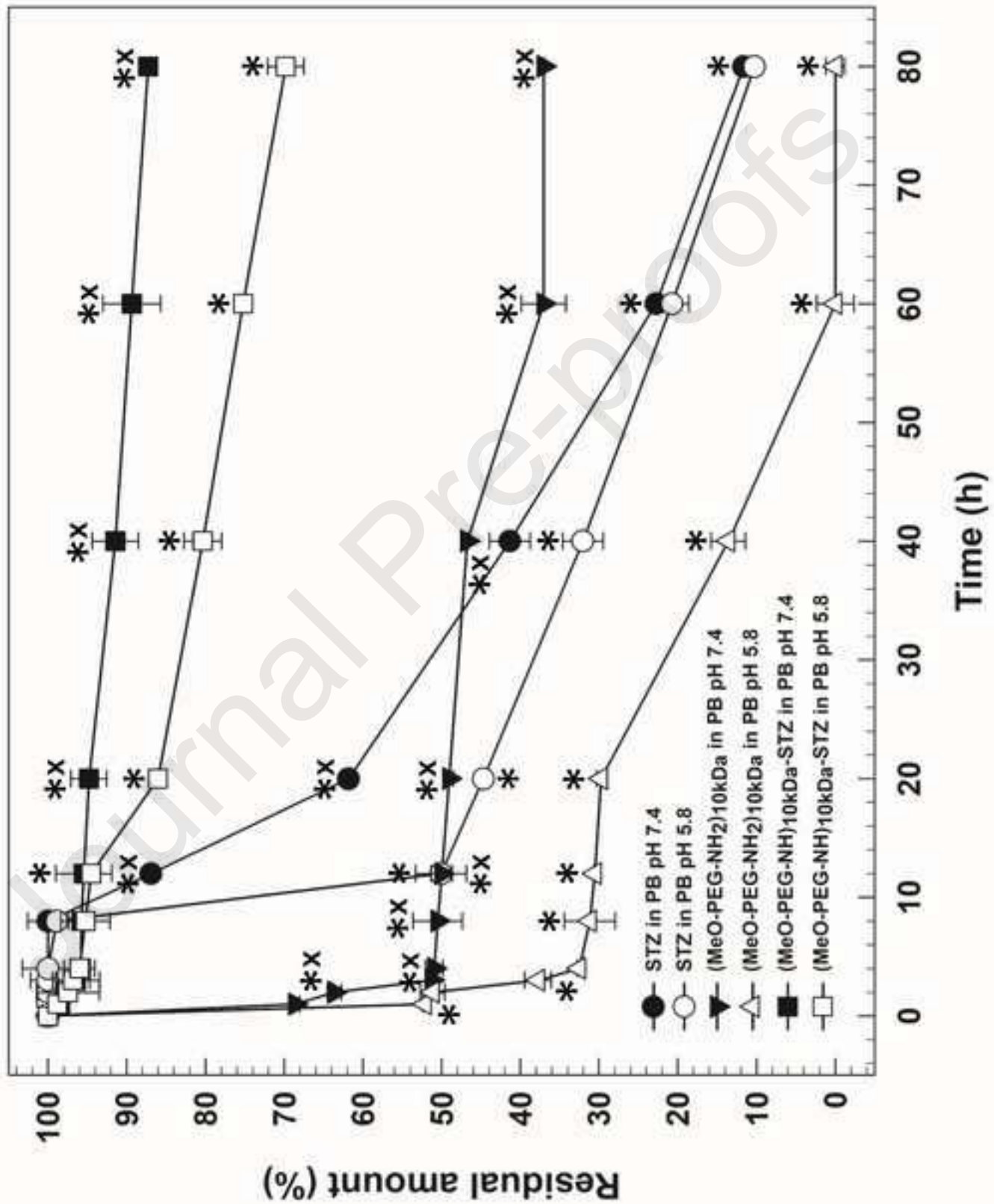

Figure 2

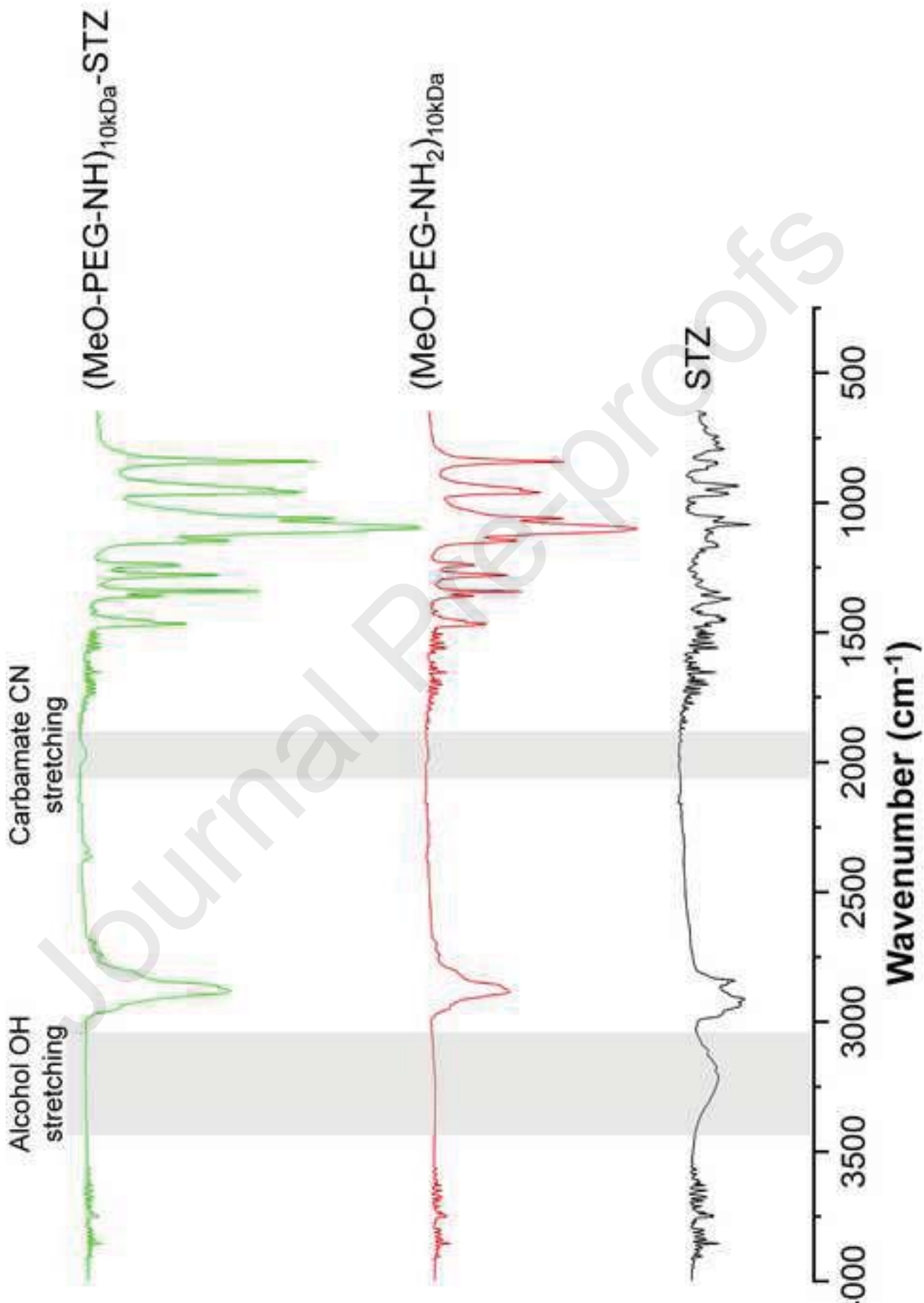

Figure 3

Figure 4

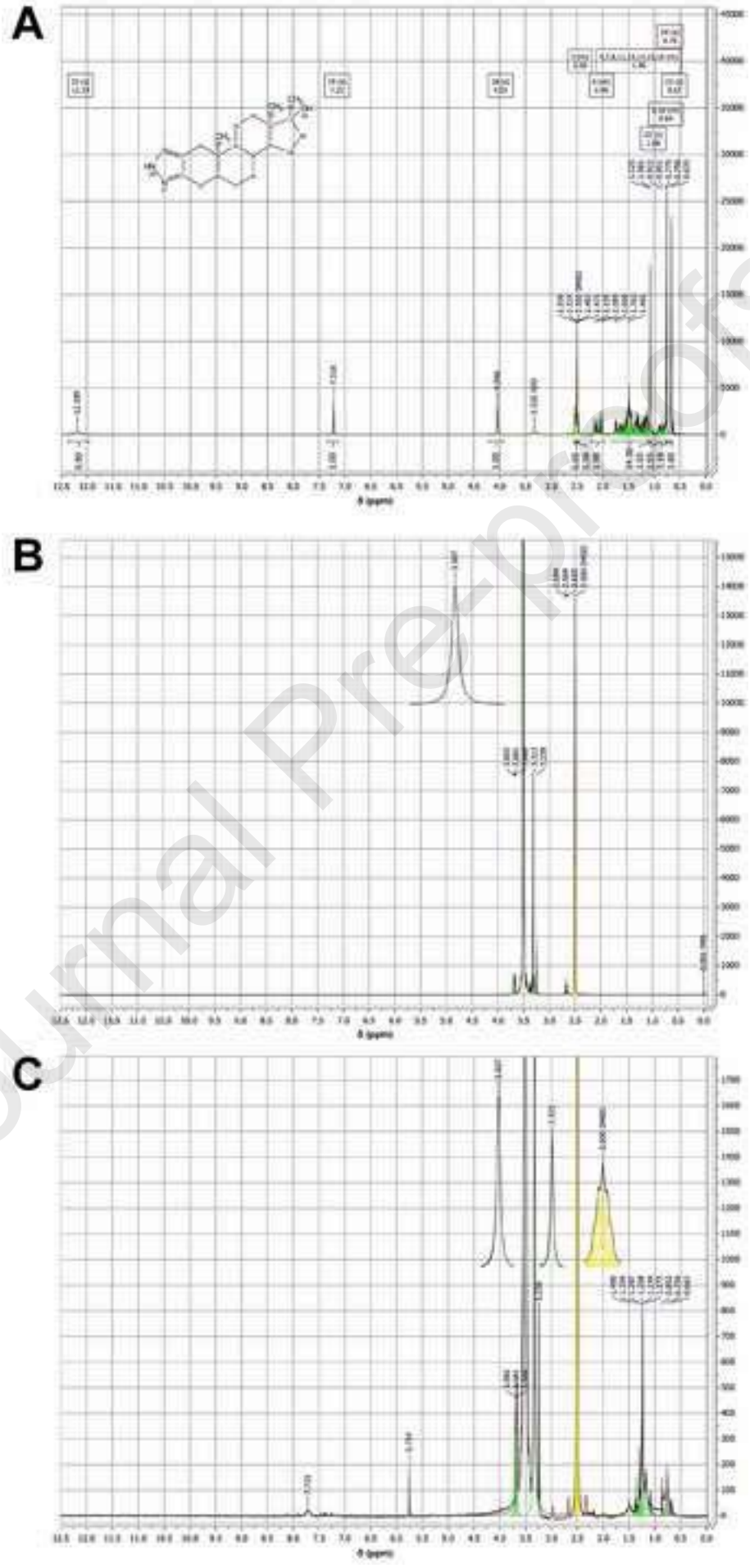

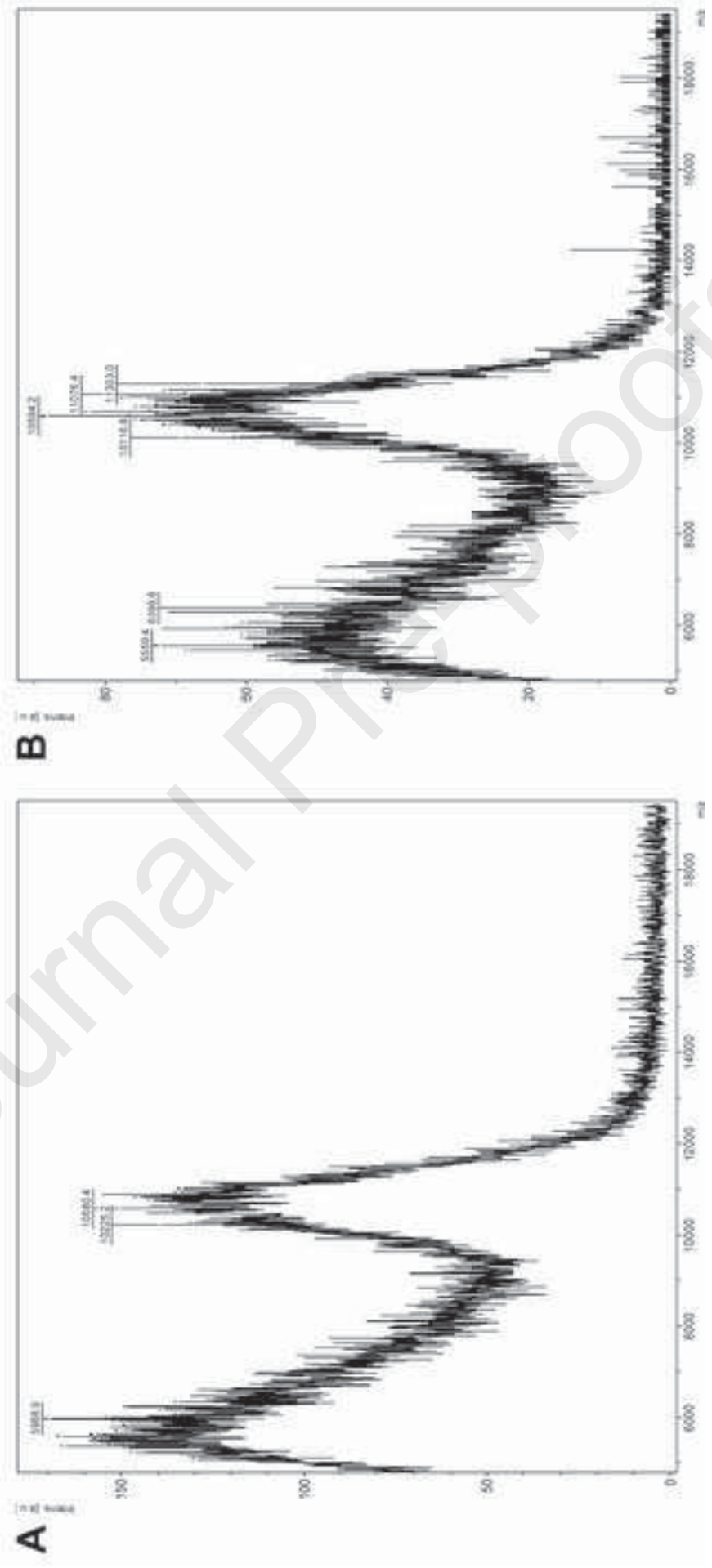

Figure 5

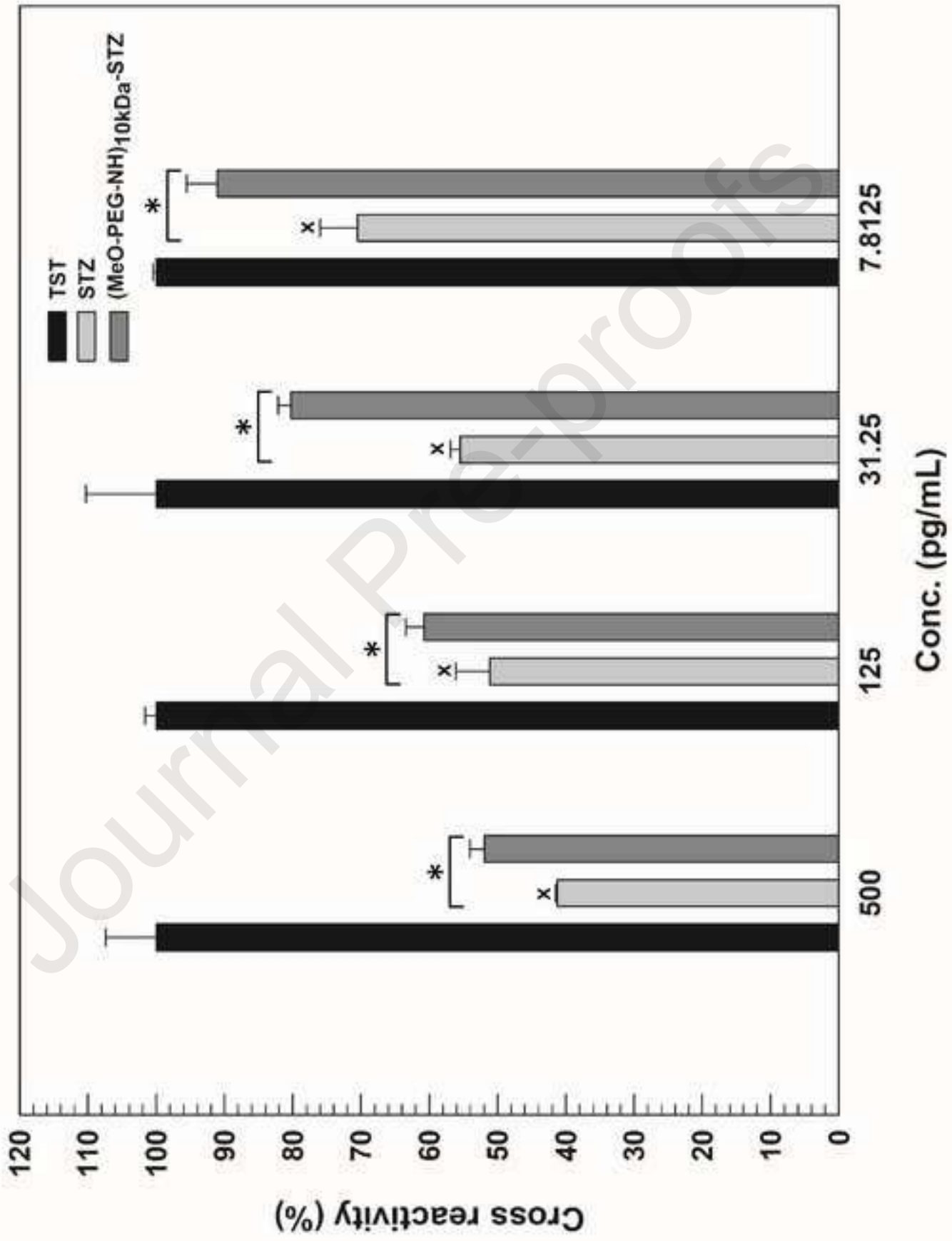

Figure 6

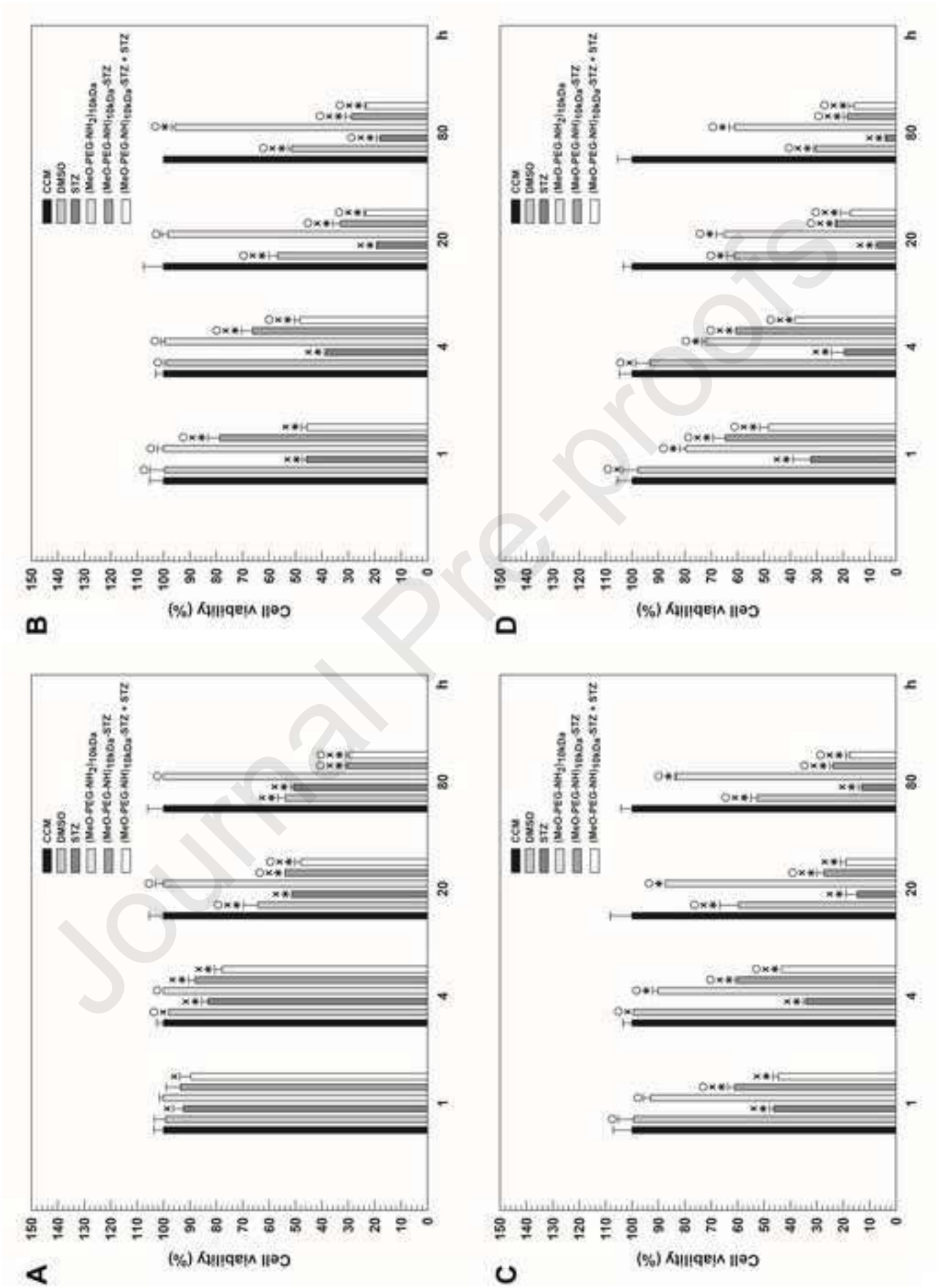

Figure 7